JACS
JOURNAL OF THE AMERICAN CHEMICAL SOCIETY

Article

pubs.acs.org/JACS

Atomic Structures and Gram Scale Synthesis of Three Tetrahedral Quantum Dots

Alexander N. Beecher,[†] Xiaohao Yang,[‡] Joshua H. Palmer,[†] Alexandra L. LaGrassa,[†] Pavol Juhas,[§] Simon J. L. Billinge,[‡,§] and Jonathan S. Owen*,[†]

[†]Department of Chemistry and [‡]Department of Applied Physics and Applied Mathematics, Columbia University, New York, New York 10027, United States

[§]Condensed Matter Physics and Materials Science Department, Brookhaven National Laboratory, Upton, New York 11973, United States

Supporting Information

ABSTRACT: Luminescent semiconducting quantum dots (QDs) are central to emerging technologies that range from tissue imaging to solid-state lighting. However, existing samples are heterogeneous, which has prevented atomic-resolution determination of their structures and obscured the relationship between their atomic and electronic structures. Here we report the synthesis, isolation, and structural characterization of three cadmium selenide QDs with uniform compositions ($Cd_{35}Se_{20}(X)_{30}(L)_{30}$, $Cd_{56}Se_{35}(X)_{42}(L)_{42}$, $Cd_{84}Se_{56}(X)_{56}(L)_{56}$; X = O_2CPh, L = H_2N-C_4H_9). Their UV-absorption spectra show a lowest energy electronic transition that decreases in energy (3.54 eV, 3.26 eV, 3.04 eV) and sharpens as the size of the QD increases (fwhm = 207 meV, 145 meV, 115 meV). The photoluminescence spectra of all three QDs are broad with large Stokes shifts characteristic of trap-luminescence. Using a combination of single-crystal X-ray diffraction and atomic pair distribution function analysis, we determine the structures of their inorganic cores, revealing a series of pyramidal nanostuctures with cadmium terminated {111} facets. Theoretical and experimental studies on these materials will open the door to a deeper fundamental understanding of structure−property relationships in quantum-confined semiconductors.

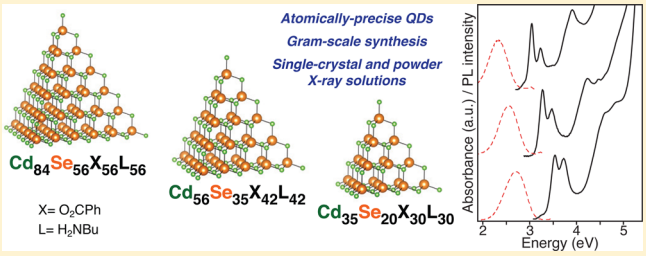

INTRODUCTION

The unique optoelectronic properties of semiconducting quantum dots (QDs) are derived from the size and structure of their inorganic cores as well as a ligand shell that provides colloidal stability and passivates surface derived electronic states.[1,2] However, a detailed understanding of the relationships between their atomic structure, optoelectronic properties, and thermodynamic stability remains elusive because atomic resolution structures are not known.

Determining the atomic structures of nanomaterials is notoriously difficult,[3] and QDs, in particular, lack exact structural solutions. Single crystal X-ray diffraction (SCXRD) has been successfully applied to certain well-defined nanomaterials,[4,5] but its applicability to less well-defined materials, including semiconducting QDs, is limited by the stringent requirement that diffraction-quality single crystals can be obtained. More widely available are powder samples of nanocrystals that are orientationally and spatially disordered. These samples produce broad, diffuse X-ray scattering features, which may contain sufficient information to allow structure determination by total scattering and atomic pair distribution function (PDF) analysis.[6,7] However, to obtain exact atomic structure solutions, these X-ray techniques require bulk samples of ordered and atomically precise materials.

Even the most monodisperse QD samples generally exhibit dispersity in composition, size, shape, and structure at the atomic level.[8] This heterogeneity results from a growth mechanism that favors no particular size.[1] There are some examples of so-called "magic-sized" CdSe clusters[9−12] whose preference for certain sizes indicates a high degree of uniformity, but whose structures remain unknown and, in some cases, are suspected to be disordered.[13,14] Another family of II-VI materials has been structurally characterized by SCXRD,[15−17] but their unusual stability is made possible by phenyl chalcogenolate ligands, which produce chalcogen rich stoichiometries and dominate their optoelectronic properties.[18,19] In contrast, most QDs have metal rich stoichiometries and surfaces bound by carboxylate, phosphonate, and/or amine ligands.[20,21] Here we report the first atomic structures of three QDs with this characteristic surface motif. This advance brings us closer to an atomically resolved understanding of the chemistry and physics of quantum-confined semiconductors.

RESULTS AND DISCUSSION

To access single-sized, atomically precise QDs, we targeted a recently discovered class of nanocrystals that exhibit strong size

Received: April 14, 2014
Published: July 8, 2014

dx.doi.org/10.1021/ja503590h | J. Am. Chem. Soc. 2014, 136, 10645−10653

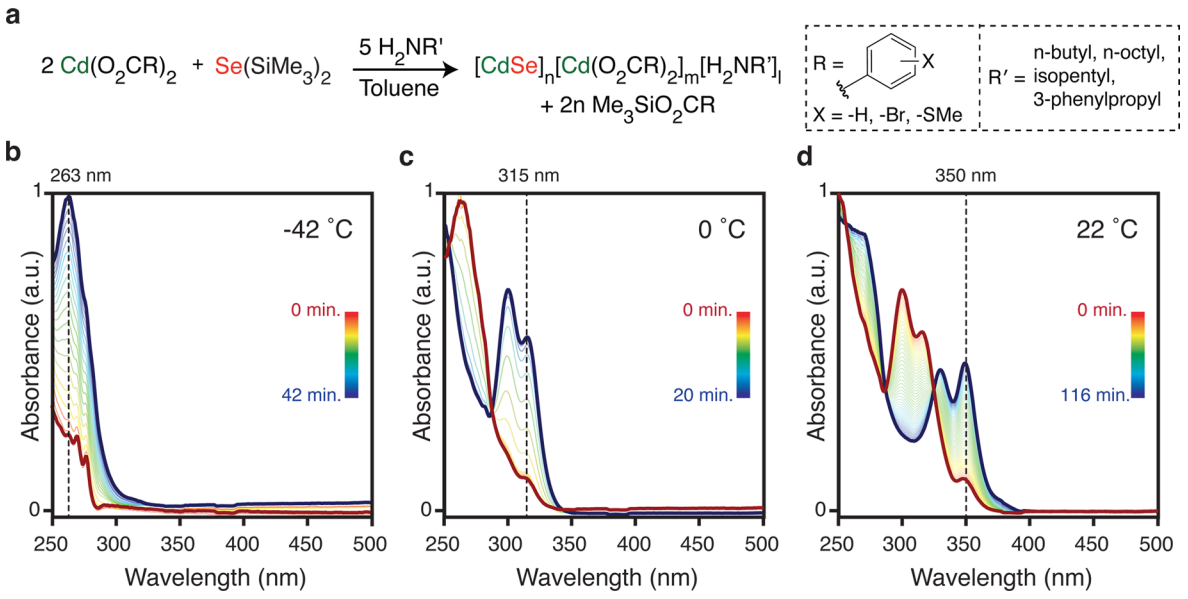

Figure 1. (a) Formation of CdSe QDs occurs upon combining $Cd(O_2CR)_2$, *n*-alkylamine, and $(TMS)_2Se$ precursors in diethyl ether at −78 °C followed by controlled warming to room temperature. (b–d) In situ monitoring of QD growth with UV–visible absorbance spectroscopy reveals isosbestic points indicating the direct conversion of smaller QDs into larger ones without the accumulation of intermediates. Spectra were measured every two minutes.

preference and grow in an unusual "quantized" manner in which small nanocrystals convert into larger ones bypassing intermediate sizes.[22] The reported syntheses of these compounds required elevated reaction temperatures (>60 °C) to effect precursor conversion, resulting in inseparable mixtures of QD sizes.[12,22,23] We discovered that a highly reactive selenium precursor, bis(trimethylsilyl)selenide ($(TMS)_2Se$), converts quantitatively into cadmium selenide upon mixing with cadmium carboxylates and primary alkylamines at room temperature or below (Figure 1a). Using ^1H nuclear magnetic resonance (NMR) spectroscopy, we observe the clean formation of the expected trimethylsilyl ester coproduct indicating complete and selective $(TMS)_2Se$ conversion at room temperature. The CdSe containing product is conveniently purified by precipitation with acetonitrile and subsequent filtration, allowing us to selectively prepare a single QD size on gram scale. A variety of carboxylates derived from sp^2-centers (e.g., substituted benzoates and furoate) and primary aliphatic amines (e.g., *n*-alkylamines and 3-phenylpropylamine) can be substituted for the standard benzoate and *n*-$BuNH_2$ ligands, while aliphatic carboxylates and bulkier amines lead to less stable structures and different growth pathways (Supporting Information Figure S1).

The high reactivity of $(TMS)_2Se$ made it possible to monitor QD formation at low temperature by in situ UV–visible absorbance spectroscopy (Figure 1b–d). As an ethereal solution of *n*-butylamine (*n*-$BuNH_2$), cadmium benzoate ($Cd(O_2CPh)_2$), and $(TMS)_2Se$ is warmed from −78 °C to −42 °C (Figure 1b), the precursors react, and the π to π^* transitions of the benzoate ligands become obscured by a much stronger absorbance from the cadmium selenide product (λ_{max} = 263 nm). This species subsequently converts into a previously unobserved species, $\mathbf{CdSe}_{(315\ nm)}$ (λ_{max} = 315 nm), at 0 °C. Further warming to room temperature transforms this QD into a larger one, $\mathbf{CdSe}_{(350\ nm)}$. Controlled conversion to larger sizes continues at higher reaction temperatures, ultimately producing QDs with dimensions of ∼3 nm.[12] The well-defined isosbestic points visible in the spectral data (Figure 1c,d) are characteristic of two families of molecules that quantitatively interconvert without the formation of strongly absorbing intermediates. Thus the component spectra are representative of single QDs. This behavior demonstrates the reaction's extraordinary selectivity for specific products that inhabit local thermodynamic minima and are therefore likely to have atomically precise structures.

Under these size-selective growth conditions, mixtures of multiple QDs are avoided, and instead, we prepare and isolate three single-sized QDs with lowest-energy electronic transitions (LEETs) at 350, 380, and 408 nm ($\mathbf{CdSe}_{(350nm)}$, $\mathbf{CdSe}_{(380\ nm)}$, and $\mathbf{CdSe}_{(408\ nm)}$). The strategy is remarkable for its simplicity: gently heating a solution of $\mathbf{CdSe}_{(350\ nm)}$ completely converts it into a mixture of $\mathbf{CdSe}_{(380\ nm)}$ and $\mathbf{CdSe}_{(408\ nm)}$ that can be trivially separated by selective precipitation. It should be noted that $\mathbf{CdSe}_{(350nm)}$ slowly grows to the next largest size when stored in solution at room temperature, particularly if the amine concentration is lower than 5 mM, suggesting a dynamic equilibrium with a coordinatively unsaturated species preceding growth.

The optical properties of these samples resemble those of conventional QDs with very small dimensions (Figure 2 and Table 1) exhibiting intense, size-dependent excitonic absorption features. The full width at half-maximum (fwhm) of the LEET decreases from 207 to 145 meV and then to 115 meV with increasing QD size, linewidths that are comparable to those of larger, relatively monodisperse QD ensembles.[24] The observed trend of increasing fwhm with decreasing size is consistent with predictions that exciton–phonon coupling is strengthened in small crystallites.[25−27] The photoluminescence (PL) of these samples is broad and substantially Stokes-shifted but nonetheless size-dependent, characteristics that are typical of small QDs.[12] Notably, larger QDs (LEET ≥ 425 nm) formed at higher temperatures using similar synthetic methods display band edge PL in addition to a broad trap-luminescence feature.[12] Thus, the large Stokes shift and broad line width of

dx.doi.org/10.1021/ja503590h | J. Am. Chem. Soc. 2014, 136, 10645−10653

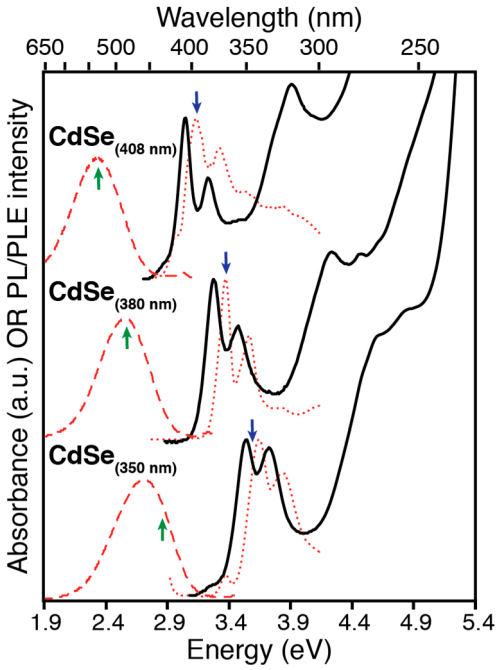

Figure 2. Absorbance (298 K, solid black lines), photoluminescence excitation (PLE, 77 K, dotted red lines) and photoluminescence (77 K, dashed red lines) spectra of purified QDs. Blue down-pointing arrows indicate the excitation wavelength for PL and green up-pointing arrows indicate the emission wavelength used for PLE measurements. A small concentration of **CdSe**$_{(380\ nm)}$ spontaneously forms from **CdSe**$_{(350nm)}$ at room temperature and is visible in the absorption and PLE spectrum of **CdSe**$_{(350nm)}$. Similarly, a small concentration of a larger size is visible in the absorption and PLE spectra of **CdSe**$_{(408nm)}$.

Table 1. Summary of QD Optical Properties

QD	1st/2nd λ max.[a] (nm)	1st/2nd abs. fwhm (meV)	PL max /Exc. λ[b] (nm)	PL fwhm[b] (meV)
CdSe$_{(350\ nm)}$	350/333	207/304	457/346	527
CdSe$_{(380\ nm)}$	380/357	145/257	484/368	471
CdSe$_{(408\ nm)}$	408/384	115/175	529/396	461

[a]To extract the fwhm, absorption spectra were expressed in eV and the regions corresponding to the lowest energy electronic transition were fitted to a Gaussian function using least-squares regression analysis. [b]Measured at 77 K.

the PL of **CdSe**$_{(350nm)}$, **CdSe**$_{(380\ nm)}$, and **CdSe**$_{(408\ nm)}$ appear to be a consequence of their very small size and are perhaps related to the strong coupling of the exciton to vibrational motions, a behavior that is typical of small molecule fluorophores and bulk materials that undergo exciton self-trapping upon distortion in the excited state.[28,29]

In order to determine the QDs' structures, we combined SCXRD and PDF analysis. Diffraction quality single crystals of **CdSe**$_{(350\ nm)}$ were grown via diffusion of acetonitrile into a solution of diethyl ether. These crystals could be redissolved to verify that the absorption spectrum is unchanged by the crystallization process. Although disorder prevented modeling of the organic ligand shell and limited structure refinement to 1.8 Å resolution, the data are sufficient to conclude that **CdSe**$_{(350\ nm)}$ is a zinc-blende tetrahedron terminated by cadmium rich {111} facets with the formula: $Cd_{35}Se_{20}$ (Figure 3 and Table S1 in the Supporting Information).

To obtain structures of **CdSe**$_{(380\ nm)}$ and **CdSe**$_{(408\ nm)}$, which did not readily form diffraction-quality single crystals, we

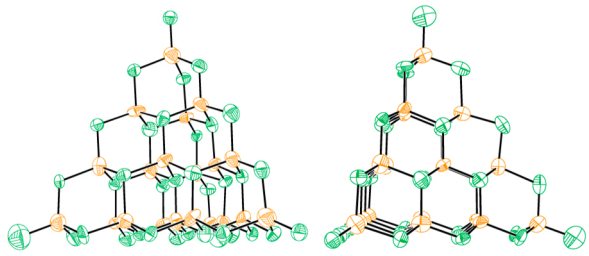

Figure 3. Two views of the $Cd_{35}Se_{20}$ core structure (Se is orange, Cd is green). Thermal ellipsoids are set at the 30% probability level.

turned to PDF analysis of total X-ray scattering from QD powders (see Experimental Section). In brief, the PDF is a weighted probability distribution of interatomic distances generated by taking a Fourier transform of the integrated scattering data. The PDFs of all three QDs are shown in Figure 4. The sharp, well-resolved peaks suggest high symmetry and a well-defined local structure. The PDF of **CdSe**$_{(350\ nm)}$ (Figure 4a), for example, exhibits sharp features to at least 1.3 nm, which is consistent with a monodisperse sample of QDs with dimensions on the order of the single crystal solution. Broad features visible at higher r originate from interparticle correlations of a relatively ordered powder.[6] As expected from the optical data, the PDFs of **CdSe**$_{(380\ nm)}$ and **CdSe**$_{(408\ nm)}$ exhibit sharp features that extend to progressively longer distances.

While ab initio determination of a structural solution from the PDF alone is a significant challenge, the SCXRD of **CdSe**$_{(350\ nm)}$ provided a candidate structural model, a zinc-blende tetrahedron with the formula $Cd_{35}Se_{20}$. A simulated PDF generated from the single crystal structure is in excellent agreement with the experimental data resulting in very low residual signal intensity across the fitted range (R_w = 0.14, fitting range = 1−20 Å). We arrived at similar structural models for **CdSe**$_{(380\ nm)}$ and **CdSe**$_{(408\ nm)}$ by hypothesizing that their structures are larger tetrahedra expanded by additional layers of atoms. Simulated PDFs of pyramids cut from the zinc-blende lattice closely match the experimental PDFs as shown in Figure 4b,c. The fits are excellent, with lower R_w values of 0.12 for **CdSe**$_{(380\ nm)}$ and 0.10 for **CdSe**$_{(408\ nm)}$ (fitting range = 1−20 Å). For comparison, previously published simulations of bulk CdSe (R_w = 0.12, fitting range = 1−40 Å), 2.4 nm CdSe nanocrystals (R_w = 0.28, fitting range = 1−40 Å), and C_{60} (R_w = 0.18, fitting range = 1−10 Å) have larger residual signals.[14] It is important to note that it is difficult to compare R_w values measured across different fitting ranges and for different materials due to the influence of systematic errors that depend upon atomic scattering factors and increase with larger fitting ranges.

To assess the reliability of our solutions, we explored other candidate structures by simulating their PDFs and comparing the magnitude of their R_w values. Very different structures, including those previously reported for bare, stoichiometric "magic-sized" clusters,[9,30−32] are easily ruled out by their qualitatively distinct PDFs and much larger R_w values (Supporting Information Figure S3). Simulated PDFs of known tetrahedral clusters with chalcogenolate surface ligands and zinc blende-like cores better reproduce the experimental data (Supporting Information Figure S4);[33,34] however, the fit is still relatively poor, which can perhaps be attributed to the clusters' chalcogen rich compositions and distorted zinc blende

dx.doi.org/10.1021/ja503590h | J. Am. Chem. Soc. 2014, 136, 10645−10653

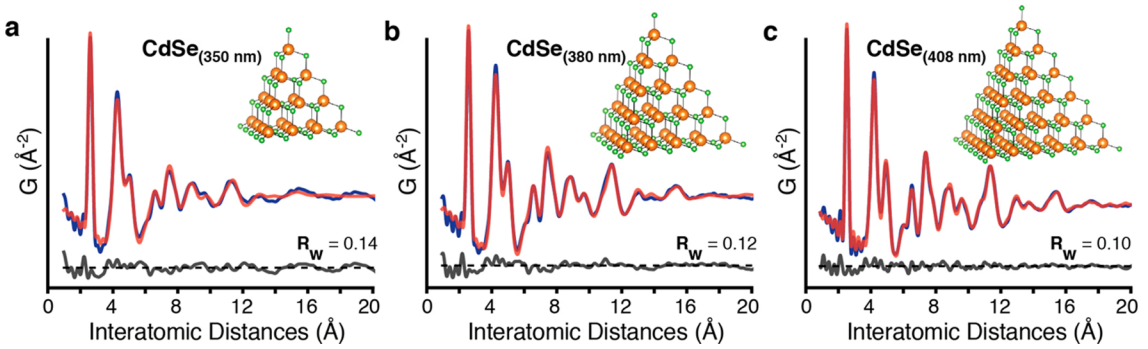

Figure 4. Experimental PDF data (blue) with simulated PDFs (red) overlaid for the three different QDs studied. The quality of the agreement is very good as shown by low residuals (black) and goodness of fit values, R_w.

structures. A series of models with more subtle differences from the tetrahedral solutions shown in Figure 4 also tested (Figure 5). Both addition and subtraction of single atoms at the edges, corners, and faces lead to poorer agreement and increased R_w. Comparisons of simulated and experimental data were made across several ranges of r (1−12 Å, 1−16 Å, 1−20 Å, 1−22 Å, and 1−25 Å) to evaluate any bias caused by inter-QD correlations at high r or correlations from organic ligands at low r that are not part of the simulation. For **CdSe**$_{(380\ nm)}$ and **CdSe**$_{(408\ nm)}$, the results unambiguously support the pristine tetrahedral structure with purely cadmium enriched surfaces including four corner Cd atoms. The consistency among different fitting ranges demonstrates the PDF results are reliable and not dominated by data collection statistics, for example. The quality of the fit for **CdSe**$_{(350\ nm)}$ depends on the fitting range, a result that might be explained by the greater contribution of inter-QD and organic ligand scattering correlations in the data. This ambiguity suggests that the information content in the PDF data alone is marginal for making this determination. However, the structure solution with all four corner atoms is preferred for several reasons: (1) The R_w minima are clustered close to this structure; (2) models of the larger QDs evaluated over all fitted ranges favor corner atoms; and (3) removing 1−3 corner atoms would lead to lower symmetry. These observations strongly support the tetrahedral assignments shown in Figure 4 for all three sizes.

Due to disorder in the single crystals and the relatively weak scattering power of the organic ligands, the combined PDF/SCXRD approach did not allow complete characterization of the molecular formula. We instead deduce the formulas of **CdSe**$_{(350nm)}$,**CdSe**$_{(380nm)}$, and **CdSe**$_{(408nm)}$ using inductively coupled plasma optical emission spectroscopy (ICP-OES), combustion analysis, infrared absorption, and nuclear magnetic resonance (NMR) spectroscopies (Table 2, Supporting Information Figures S5 and S6). The Cd:Se ratios measured by ICP-OES are consistent with the structures determined by X-ray diffraction. The Cd:Se ratio fixes the benzoate content because each cadmium in excess of selenium must be charge-balanced by two benzoate anions to arrive at a neutral QD-ligand complex. The ^{1}H NMR spectra of each QD shows that the number of *n*-butylamine ligands is equal to the number of benzoate ligands within the 10% uncertainty of the integration. Thus, in the case of **CdSe**$_{(350\ nm)}$, the 15 excess cadmiums are balanced by 30 benzoate anions and an additional 30 ± 3 *n*-$BuNH_2$ ligands. This line of reasoning yields the chemical formulas $Cd_{35}Se_{20}(O_2CAr)_{30}(H_2NR)_{30}$ for **CdSe**$_{(350\ nm)}$, $Cd_{56}Se_{35}(O_2CAr)_{42}(H_2NR)_{42}$ for **CdSe**$_{(380\ nm)}$, and

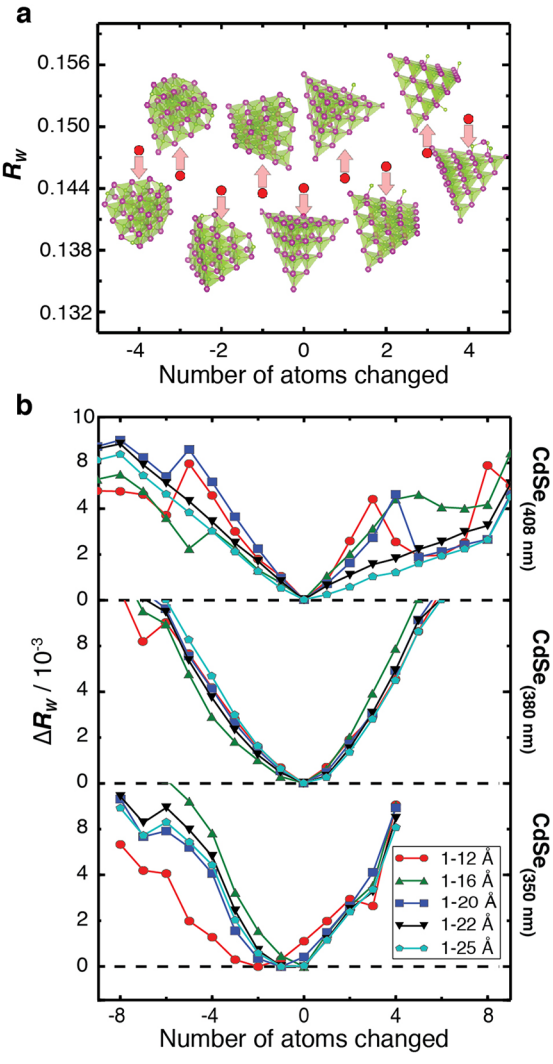

Figure 5. PDF structure modeling. (a) Atomic structure models of **CdSe**$_{(350\ nm)}$ and their agreement factor (R_w) to the experimental data across the range r = 1−20 Å. The Cd and Se atoms are colored in magenta and green, respectively. (b) Change in R_w for **CdSe**$_{(350\ nm)}$ (bottom), **CdSe**$_{(380\ nm)}$ (middle), and **CdSe**$_{(408\ nm)}$ (top) as a function of single atom additions/subtractions to the pristine tetrahedron. Five different fitting ranges were evaluated: 1−12 Å (red dots), 1−16 Å (green up-pointing triangles), 1−20 Å (blue squares), 1−22 Å (black down-pointing triangles), and 1−25 Å (turquoise pentagons). ΔR_w is calculated relative to the best fitting model, which is generally the pristine tetrahedron ($\Delta R_w = R_w - R_{w(min)}$).

dx.doi.org/10.1021/ja503590h | J. Am. Chem. Soc. 2014, 136, 10645−10653

Table 2. Summary of QD Structural Properties

QD	chemical formula	edge length (nm)	coord. sites	# of ligands[a]	ICP-OES. Cd:Se ratio[b]	theor. Cd:Se ratio	measured % mass C	theor. % mass C
CdSe$_{(350\ nm)}$	$Cd_{35}Se_{20}(O_2CPh)_{30}(H_2NR)_{30}$	1.71	60	60	1.71 ± 0.14	1.75	32.92	34.90
CdSe$_{(380\ nm)}$	$Cd_{56}Se_{35}(O_2CPh)_{42}(H_2NR)_{42}$	2.14	84	84	1.61 ± 0.17	1.60	31.63	32.19
CdSe$_{(408\ nm)}$	$Cd_{84}Se_{56}(O_2CPh)_{56}(H_2NR)_{56}$	2.57	112	112	1.53 ± 0.06	1.50	27.96	29.87

[a]Uncertainty in individual measurements of amine content is 10% due to the difficulty of accurately integrating the broad NMR signals. Repeated measurements support a 1:1 amine to benzoate ratio for each QD (**CdSe$_{(350\ nm)}$** average ratio 1.045 with a standard deviation of 0.050; **CdSe$_{(380\ nm)}$** average ratio 1.025 with a standard deviation of 0.066). [b]Determinations of cadmium and selenium content were made by inductively coupled plasma optical emission spectroscopy (ICP-OES). **CdSe$_{(350\ nm)}$** was measured a total of five times. **CdSe$_{(380\ nm)}$** and **CdSe$_{(408\ nm)}$** were each measured three times.

$Cd_{84}Se_{56}(O_2CAr)_{56}(H_2NR)_{56}$ for **CdSe$_{(408\ nm)}$**. However, a range of ligand compositions is possible and cannot be ruled out given the scatter in the elemental analysis data.

The number of ligands found on each QD matches the number of vacant coordination sites assuming four-coordinate cadmium centers and monodentate benzoate coordination. On a cadmium selenide {111} facet, the density of coordination sites (6.2 sites/nm^2) is higher than the packing density of crystalline alkane chains (4.9 chains/nm^2) and the binding of one ligand to each coordination site over large areas is unlikely.[35,36] On these small, tetrahedral QDs, however, the effective curvature increases the volume available to the ligand shell by 2−3 times relative to a planar surface of equivalent area (Supporting Information Table S2). Using our measured formulas, we estimate that the density of ligand atoms (C, H, N, O) increases from 80 atoms/nm^3 to 90 atoms/nm^3 as the tetrahedron increases in size and the effective curvature decreases. These densities are lower than what is found in typical crystalline alkylammonium benzoate salts (~105 atoms/nm^3) indicating that the proposed chemical formulas are not limited by the packing density of ligands despite their high coverage (see Supporting Information for additional discussion). One ligand on every coordination site leads to a surface without dangling bonds, perhaps explaining the special stability of these structures. This high ligand density further supports the hypothesis that the photoexcited QD reorganizes according to the Franck−Condon principle rather than radiating from a distribution of luminescent midgap excitonic states.[28,29]

Knowledge of each QD's structure allows us to precisely analyze the size-dependence of the band gap at these unusually small sizes. By plotting an effective radius against the energy of the LEET for both our QDs and previously reported QDs,[37] we observe a nearly identical size dependence in the two sample sets (Figure 6). We fit the combined data sets to a fourth-order polynomial to generate a sizing curve that is nearly identical to the one determined previously,[37] but better supported at energies greater than 3 eV.

The atomically precise compositions of **CdSe$_{(350\ nm)}$**, **CdSe$_{(380\ nm)}$**, and **CdSe$_{(408\ nm)}$** made their structural solution possible. In a few cases, the formulas and calculated structures of other cadmium selenide species that adopt preferred sizes have been assigned on the basis of laser-desorption ionization mass spectrometry (LDI-MS) measurements.[9,32,38] Among the range of species observed in these spectra, $(CdSe)_{13}$, $(CdSe)_{19}$, $(CdSe)_{33}$, and $(CdSe)_{34}$ are found in greatest abundance.[9] However, this technique produces the same fragments from much larger nanocrystals and bulk CdSe.[9,22,23] Indeed, LDI-MS studies of **CdSe$_{(350\ nm)}$** also produce signals from $(CdSe)_{13}$, $(CdSe)_{19}$, $(CdSe)_{34}$, and other fragments (see Supporting Information Figure S7 and S8). The lack of organic ligands suggests that these fragments result from the special stability of gas-phase clusters formed by laser ablation rather than ones stabilized in solution. In contrast, the stability of **CdSe$_{(350\ nm)}$**, **CdSe$_{(380\ nm)}$**, and **CdSe$_{(408\ nm)}$** is a consequence of their surface termination and the high ligand coverage; at these sizes, a tetrahedron is uniquely suited to minimize the number of unfilled coordination sites per surface atom while simultaneously maintaining a low surface-area-to-volume ratio.

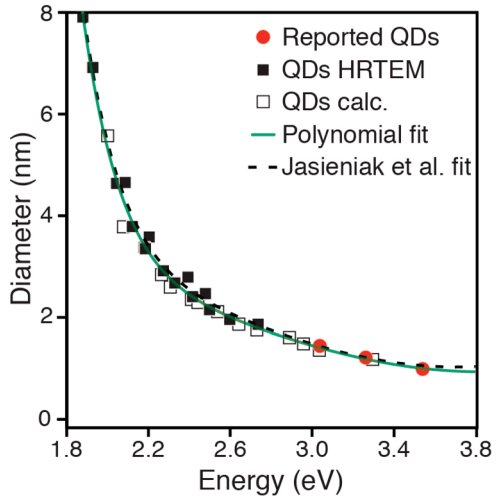

Figure 6. Our QDs (red circles) exhibit very similar size dependence to the experimental (solid squares) and calculated (open squares) results used by Jasieniak et al. to create a sizing curve. Merging our two data sets yields a new empirical sizing relationship $d_{(nm)} = 49.9019 - (0.470699)\lambda + (1.66480 \times 10^{-3})\lambda^2 - (2.57705 \times 10^{-6})\lambda^3 + (1.49956 \times 10^{-9})\lambda^4$ (green, solid line) that is similar to the relationship found by Jasieniak et al. (black, dashed line), but better supported in the small size regime.[37]

CONCLUSION

The reported structures and formulas provide a direct view into the origins of QD stability and optical properties without ambiguities from distributions of crystal sizes and shapes and/or electronic transitions associated with the ligand shell. The dynamic nature of these materials is remarkable; complex, pyramidal structures form rapidly at low temperatures and readily convert into larger QDs without accumulation of intermediate structures. In addition, we demonstrate the power of PDF methods for determining the structure of homogeneous nanomaterials. This approach holds great promise for atomic structure solutions generally, and particularly as ab initio structure-searching methods develop. Studies of this kind will enable detailed experimental and first-principle investigations into the relationship between geometric and electronic structure on the nanoscale.

EXPERIMENTAL SECTION

General Considerations. Benzoic acid (≥99.5%), benzoic anhydride, dichloromethane (≥99.5%), selenium pellets (≥99.99%), Superhydride solution (1.0 M lithium triethylborohydride in tetrahydrofuran), and tetrahydrofuran (≥99.0%) were purchased from Sigma Aldrich and used as received. Benzene-d_6 (99.6%) and anhydrous acetonitrile (99.5%) were purchased from Sigma Aldrich, shaken with activated alumina, filtered, and stored over 4 Å molecular sieves for at least 24 h prior to use. Diethyl ether, pentane, and toluene were dried over alumina columns and stored over 4 Å molecular sieves for at least 24 h prior to use. Bromotrimethylsilane (97%), *n*-butylamine (99%), *n*-octylamine, and tetramethylethylenediamine (TMEDA) were purchased from Sigma Aldrich and dried over calcium hydride, distilled, and stored in a nitrogen glovebox. Methanol-d_4 was purchased from Cambridge Isotope Laboratories and used as received. Dimethylcadmium was purchased from Strem, vacuum distilled before use, and stored in a nitrogen atmosphere glovebox. *CAUTION: Dimethylcadmium is an extremely toxic liquid and due to its volatility and air-sensitivity should only be handled by a highly trained and skilled scientist.*

Unless otherwise indicated, all manipulations were performed under air-free conditions using standard Schlenk techniques or a nitrogen atmosphere glovebox. NMR spectra were recorded on Bruker Avance III 400 and 500 MHz instruments and internally referenced to the resonances of protio-impurities in the deuterated solvent. ^{1}H NMR spectra were acquired with sufficient delay to allow complete relaxation between pulses (15 s). Coupling constants are reported in hertz. UV−visible absorption data were obtained using a Perkin-Elmer Lambda 650 spectrophotometer equipped with deuterium and tungsten halogen lamps. In situ absorbance measurements were performed using a fiber optic dip probe. Photoluminescence and photoluminescence excitation spectra were recorded using a FluoroMax-4 from Horiba Scientific. Diffuse Reflectance Infrared Fourier Transform Spectroscopy (DRIFTS) was performed on a Nicolet 6700 FT-IR from Thermo Fisher equipped with a Harrick Praying Mantis Diffuse Reflection Accessory.

Synthesis and Isolation of Cadmium Benzoate ($(Cd(C_7H_5O_2)_2)_3(CH_3CN)_1$). To a Schlenk flask, cadmium oxide (18.11 g, 141 mmol), benzoic acid (103.31 g, 846 mmol), and benzoic anhydride (38.23 g, 169 mmol) are added, and the flask is sealed under vacuum. The red-brown mixture is heated with stirring to 180 °C to achieve a colorless melt, which resolidifies as the mixture is cooled to room temperature. Excess benzoic acid and benzoic anhydride are removed by washing the solid on a fritted funnel with toluene (3 × 200 mL toluene) and then dichloromethane (2 × 200 mL dichloromethane). The resulting powder is dissolved in a mixture of 100 mL tetrahydrofuran and 200 mL acetonitrile and concentrated by distillation with heat causing a milky white solid to precipitate. The cooled suspension is filtered and the powder dried under vacuum at 100 °C overnight to yield 24.75 g (47.7%) of free flowing white powder. The product is insoluble or sparingly soluble in most common organic solvents with the exceptions of coordinating solvents such as tetrahydrofuran, 1,4-dioxane, and benzonitrile. Single crystals suitable for X-ray crystallography were grown upon cooling a saturated acetonitrile/tetrahydrofuran (~95:5) solution (see Figure S9 and Table S4 in the Supporting Information). Solutions in benzene-d_6 were prepared for analysis by ^{1}H NMR spectroscopy by adding 2 equiv of *n*-butylamine. ^{1}H NMR (400 MHz, C_6D_6): δ = 0.66 (t, $^3J_{H\text{-}H}$ = 7, 6H, Me), 0.73 (s, ACN, -CH_3), 1.00 (m, 4H, -CH_2-), 1.18 (m, 4H, -CH_2-), 2.61 (s, 4H, -NH_2), 2.67 (t, $^3J_{H\text{-}H}$ = 7, 4H, -CH_2-), 7.21 (t, $^3J_{H\text{-}H}$ = 7, 2H, Ar-H), 7.28 (t, $^3J_{H\text{-}H}$ = 7, 4H, Ar-H), 8.55 (d, $^3J_{H\text{-}H}$ = 8, 4H, Ar-H) ppm. ^{13}C{^{1}H} NMR (125.8 MHz, C6D6): δ = 0.29 (ACN, -CH_3), 13.92 (-CH_3), 20.15 (-CH_2-), 35.28 (-CH_2-), 42.53 (-CH_2-), 128.21 (*m*-Ar), 130.63 (*o*-Ar), 131.05 (*p*-Ar), 136.44 (1-Ar), 174.31 (-CO_2-) ppm. Anal. Calcd for $Cd_3C_{44}H_{33}O_{12}N$: C, 47.83; H, 3.01; N, 1.27. Found: C, 47.77; H, 3.08; N, 1.18.

Synthesis and Isolation of Other Cadmium Carboxylates. Cadmium *bis*(4-thiomethylbenzoate), cadmium *bis*(4-bromobenzoate), and cadmium *bis*(furoate) are prepared from the desired carboxylic acid and dimethylcadmium following a procedure adapted from Hendricks et al.[39] Briefly, in a nitrogen filled glovebox and in the dark, 1.98 equiv of the carboxylic acid are dissolved in tetrahydrofuran to which 1 equiv of dimethylcadmium is added dropwise. Vigorous bubbling occurs and the solution is stirred for 30 min. The solvent is distilled off under vacuum leaving a white powder, which is then dried overnight under vacuum at 100 °C.

Synthesis and Isolation of *bis*(trimethylsilyl)selenide ($Se(Si(CH_3)_3)_2$). The following two-step procedure is a variation on the one pot method reported by Detty and Seidler that proved more reliable and higher yielding.[40]

Synthesis and Isolation of Lithium Selenide (Li_2Se). In a Teflon sealed Schlenk tube under argon, lithium triethylborohydride in tetrahydrofuran (100 mL, 1 M) is chilled to 0 °C, and selenium pellets (3.91 g, 49.5 mmol) are added. The mixture is allowed to warm to room temperature and stirred for an hour resulting in a cloudy, white suspension. Tetrahydrofuran and triethylborane are removed by distillation under vacuum (*CAUTION: Triethylborane is extremely flammable and should be carefully quenched prior to disposal*), and the resulting white solid is triturated with pentane (50 mL) and collected on a fine glass frit in the glovebox. The white powder is then washed with toluene (50 mL) followed by diethyl ether (50 mL) and then dried under reduced pressure at 150 °C taking care to avoid losing the very fine white powder upon evacuation. (4.28 g; 46 mmol, 93.4% yield). It is important to carefully protect lithium selenide from oxygen to obtain a pure, colorless product. A known quantity of the powder and an internal standard (*N,N,N′,N′*-tetramethylethylenediamine) are dissolved in methanol-d_4 to check for the presence of organic impurities by ^{1}H NMR spectroscopy; typical syntheses produced a product that is >98% free from tetrahydrofuran or ethyl containing impurities.

Synthesis and Isolation of *bis*(trimethylsilyl)selenide ($Se(Si(CH_3)_3)_2$). To a nitrogen filled Schlenk tube containing lithium selenide (4.50 g, 48.5 mmol), bromotrimethylsilane (14.47 g, 94.52 mmol) is added via syringe. The suspension is degassed using the freeze−pump−thaw technique, sealed under vacuum, and heated to 100 °C for 24 h. The flask is then attached to a bulb-to-bulb, vacuum transfer apparatus and a clear, colorless oil is distilled from the suspension with the help of a heat gun (8.54 g; 37.9 mmol; 80.2% yield). If necessary, residual bromotrimethylsilane or hexamethyldisiloxane can be removed by partial vacuum distillation (45 °C, 20 Torr) leaving pure $Se(Si(CH_3)_3)_2$. In the event that accidental contamination of the reaction mixture or the starting material with oxygen occurs, an impure yellow product is obtained upon distillation. This material should be purified by addition of tri-*n*-octylphosphine and redistillation prior to long-term storage. ^{1}H NMR (C_6D_6, 400 MHz): δ = 0.38. ^{13}C{^{1}H} NMR (125.8 MHz, C_6D_6): δ = 4.65 (-CH_3) ppm.

Synthesis and Isolation of $CdSe_{(350\ nm)}$. Cadmium benzoate (2.00 g, 5.43 mmol) and *n*-butylamine (0.993 g, 13.58 mmol) are dissolved in diethyl ether (20 mL), and the solution is cooled to 0 °C in an ice water bath. In a separate flask, a solution of *bis*(trimethylsilyl)selenide (0.612 g, 2.72 mmol) and diethyl ether (20 mL) is cooled to 0 °C and then cannula-transferred into the cadmium precursor solution. The mixture is allowed to warm to room temperature. After stirring for 30 min, the reaction mixture is concentrated under reduced pressure, and the flask is brought into the glovebox. The sticky white solid is triturated with acetonitrile (10 mL) and the powder is collected by centrifugation (3 min at 7000 rpm). After decanting the supernatant, the pellet is dissolved in a minimal amount of diethyl ether (<5 mL), reprecipitated with acetonitrile (10 mL), and again collected by centrifugation. This process is repeated once more. The purified product is dried from ether under vacuum overnight at room temperature to obtain 1.02 g of fine white powder. ^{1}H NMR (500 MHz, C_6D_6): δ = 0.60 (br, 3H, Me), 0.99 (br, 2H, -CH_2-), 1.36 (br, 2H, -CH_2-), 2.98 (br, 2H, -NH_2), 4.18 (br, 2H, -CH_2-), 7.06 (br, 2H, Ar-H), 7.28 (br d, 1H, Ar-H), 8.15 (br, 2H, Ar-H) ppm. ^{13}C{^{1}H} NMR (125.8 MHz, C_6D_6): δ = 13.88 (-CH_3), 20.19 (-CH_2-), 34.85 (-CH_2-), 42.78 (-CH_2-), 130.85 (Ar), 131.11 (Ar),

dx.doi.org/10.1021/ja503590h | J. Am. Chem. Soc. 2014, 136, 10645−10653

135.63 (Ar), 174.54 (-CO_2-) ppm. Anal.: act. 32.92, 4.55, 3.43; theo. 34.90, 4.23, 3.70.

Synthesis and Isolation of $CdSe_{(380\ nm)}$ and $CdSe_{(408\ nm)}$. Under argon, $CdSe_{(350\ nm)}$ (500 mg) is dissolved in toluene (35 mL) producing a colorless solution. After heating at 85 °C for 30 min, a yellow precipitate forms. The suspension is brought into the glovebox and centrifuged, separating the yellow $CdSe_{(408\ nm)}$ precipitate by centrifugation. The supernatant containing $CdSe_{(380\ nm)}$ is decanted and the yellow pellet is washed with toluene to remove remaining $CdSe_{(380\ nm)}$. The supernatant is concentrated to dryness under vacuum, the residue triturated with acetonitrile (10 mL), and the solids collected by centrifugation. Both samples are dried under vacuum at room temperature yielding 264 mg of $CdSe_{(380\ nm)}$ and 174 mg of $CdSe_{(408\ nm)}$. Solutions of $CdSe_{(408\ nm)}$ in benzene-d_6 were prepared for analysis by ^{1}H NMR spectroscopy by performing a ligand exchange to replace native *n*-butylamine ligands with *n*-octylamine ligands. In brief, the ligand exchange is accomplished by dissolution of $CdSe_{(408\ nm)}$ in a 10 mM solution of *n*-octylamine in toluene, followed by precipitation with acetonitrile, and centrifugation. The pellet is submitted to this process twice more before drying the product under vacuum. ^{1}H NMR $CdSe_{(380\ nm)}$ (500 MHz, C6D6): δ 0.64 (br, 3H, Me), 1.05 (br, 2H, -CH_2-), 1.42 (br, 2H, -CH_2-), 3.02 (br, 2H, -NH_2), 3.94 (br, 2H, -CH_2-), 7.02 (br, 2H, Ar-H), 7.11 (br, 1H, Ar-H), 8.08 (br, 2H, Ar-H) ppm. ^{1}H NMR $CdSe_{(408\ nm)}$ (400 MHz, C_6D_6): δ 0.91 (br, 3H, Me), 1.11 (br d, 10H, -CH_2-), 1.26 (br, 2H, -CH_2-), 2.99 (br, 2H, -NH_2), 4.08 (br, 2H, -CH_2-), 7.15 (br, 3H, Ar-H), 8.15 (br, 2H, Ar-H) ppm. C,H,N analysis of $CdSe_{(380\ nm)}$: act. 31.63, 3.99, 2.88; theo. 32.19, 3.90, 3.42. C,H,N analysis of $CdSe_{(408\ nm)}$: act. 27.96, 3.30, 2.37; theo. 29.87, 3.62, 3.17.

In Situ UV−vis Absorption. In situ UV−visible absorption data (Figure 1b−d) were collected using a Perkin-Elmer Lambda 650 UV−vis spectrometer equipped with a Mono-Fiber Transfer-Optic that redirects the beam into a fiber optic dip probe. Under nitrogen, a 100 mL three-neck flask fitted with a dip probe adapter, argon inlet, and a thermocouple adapter is charged with an ethereal solution (60 mL) of $Cd(O_2CPh)_2$ (2.18 mM) and *n*-$BuNH_2$ (5.46 mM). This solution is chilled to −78 °C and a solution of TMS_2Se in ether (15 mL, 4.37 mM) is added dropwise with vigorous stirring. The temperature is raised to −42 °C by submerging the flask in an acetonitrile dry ice bath. Spectra were recorded from 250 to 500 nm every two minutes. After the growth of a signal at 263 nm reaches completion, the temperature is raised to 0 °C by submerging the flask in an ice water bath. After the growth of signals at 315 and 300 nm reach completion, the temperature is raised to 22 °C.

Empirical Sizing Formula Determination. Data for our quantum dots (QDs) were combined with data from Jasieniak et al. and then fit to a fourth-order polynomial (diameter in nanometers as a function of position of the lowest energy electronic transition in units of nanometers) using least-squares regression analysis.[37] We modeled the volume of our QDs by summing the volumes of all Cd^{2+} and Se^{2-} ions (ionic radii of 109 and 184 pm respectively).[41] These volumes were used to calculate the radius of a sphere with an equivalent volume.

Single Crystal X-ray Diffraction. *Collection and Refinement Strategy.* Single crystal X-ray diffraction (SCXRD) data were collected on a Bruker Apex II diffractometer, and crystal data, data collection, and refinement parameters are summarized in Supporting Information Table S1. The structures were solved using direct methods and standard difference map techniques, and were refined by full-matrix least-squares procedures on F^2 with SHELXTL (Version 2008/4).[42,43] All atoms not found and refined were treated as a diffuse contribution to the electron density without specific atomic positions using SQUEEZE/PLATON.[44,45]

Unit Cell and Space Group Determination. Data were first integrated and processed using the primitive reduced cell found in APEX2, and the initial solution was transformed to the space group *Cmcm* using PLATON. At this point, the data were reintegrated using the C-centered orthorhombic unit cell reported in Supporting Information Table S1, and structure refinement was performed.

Core Structure Determination. Least-squares refinement led initially to the $Cd_{31}Se_{20}$ core solution shown in Supporting Information Figure S2a, which has an R_1 of 0.1969 after SQUEEZE is applied. Additional modeling of residual electron density in the $Cd_{31}Se_{20}$ core prior to the application of SQUEEZE leads to the $Cd_{35}Se_{20}$ core solution (Supporting Information Figure S2b), which has a lower R_1 of 0.1822 after SQUEEZE is applied. Anisotropic refinement with the ISOR restraint was applied to all atoms. Additional *Q* peaks could be observed near the surface of the $Cd_{35}Se_{20}$ core structure, but attempts to model this density were unsuccessful.

Modeling Organic Moieties. It was not possible to model organic moieties in the unit cell. This has been observed previously in metal chalcogenide single crystals and has been attributed to gross disorder.[46,47] The SQUEEZE procedure in PLATON finds large void spaces in the unit cell filled with electron density. For the $Cd_{31}Se_{20}$ core, SQUEEZE calculates a residual void volume of 52,746 Å^3, containing 21,766 electrons; for the $Cd_{35}Se_{20}$ core, SQUEEZE calculates a residual void volume of 52,461 Å^3, containing 20,732 electrons.

Powder X-ray Diffraction and Pair Distribution Function Analysis. X-ray powder diffraction experiments were performed on the X17A beamline at the National Synchrotron Light Source (NSLS) at Brookhaven National Laboratory. Diffraction data were collected using the rapid acquisition pair distribution function (RA-PDF) technique at 100 K with an X-ray energy of 38.872 keV.[48] A Perkin-Elmer flat-panel 2D detector was used for data collection with a sample distance of 118.269 mm. The diffraction pattern of a Ni metal standard was measured to calibrate detector geometry, and the scattering signal of an empty Kapton tube was measured and subtracted as the background. The 2D diffraction pattern was integrated to give 1D diffraction intensity in *q*-space using the SrXplanar program[49] and transformed into the PDF using PDFgetX3.[50]

The atomic PDF $G(r)$ describes the probability of finding atom pairs at a certain distance, *r*. Experimentally, the PDF is a sine Fourier transformation of powder diffraction data using

$$G(r) = \frac{2}{\pi}\int_{Q_{min}}^{Q_{max}} Q[S(Q) - 1]\sin Qr\ \mathrm{d}Q$$

where *Q* is the magnitude of the scattering vector, and $S(Q)$ is the total scattering function. $S(Q)$ is generated by normalizing and correcting the coherent scattering intensity $I_c(Q)$ using

$$S(Q) = \frac{I_c(Q) - \langle f^2\rangle}{\langle f\rangle^2} + 1$$

where *f* is the X-ray scattering factor averaged over all elements in the sample. Q_{min} = 0.8 Å^{-1} and $Q_{max\ x}$ = 22.5 Å^{-1} are limits placed on the *Q* range in the PDF transformation. The minimum value is determined by the beamstop, and the maximum value is chosen to reduce noise originating in the high-*Q* region.

Theoretically, the PDF can be calculated from an atomic structural model:

$$G(r) = \frac{1}{Nr}\sum_{i\neq j}\frac{f_i f_j}{\langle f\rangle^2}\delta(r - r_{ij})$$

where the Dirac delta function is expanded to a Gaussian-like function after including thermal parameters.[51] We used SrFit to optimize the parameter set giving a structural model whose PDF is most consistent with the experimental PDF. The quality of the fit is characterized by the residual function

$$R_w = \sqrt{\frac{\sum_{i=1}^{N}[G_{obs}(r_i) - G_{calc}(r_i;\vec{\mathbf{P}})]^2}{\sum_{i=1}^{N}G_{obs}^2(r_i)}}$$

where G_{obs} is the experimental PDF, G_{calc} is the calculated PDF, and $\vec{\mathbf{P}}$ is the set of refinable parameters used in the structure model.

dx.doi.org/10.1021/ja503590h | J. Am. Chem. Soc. 2014, 136, 10645−10653

The atomic structures of the QDs reported here are cut from the CdSe zincblende lattice to a tetrahedral shape with optional addition or removal of atoms from the corners or edges. Identical isotropic atomic displacement parameters (U_{iso}) are assigned for all atoms of a particular element in a given structure. To optimize fits, we refined U_{iso} and the lattice parameters of the base zincblende lattice.

■ ASSOCIATED CONTENT

Supporting Information

UV−vis measurements of QD derivatives, stability, and stoichiometry, SCXRD solutions, crystal refinement data, PDF models of previously reported CdSe materials, ^{1}H NMR, and DRIFTS measurements, a discussion of ligand packing on a tetrahedron, and MALDI-MS data. This material is available free of charge via the Internet at http://pubs.acs.org.

■ AUTHOR INFORMATION

Corresponding Author

*E-mail: jso2115@columbia.edu.

Author Contributions

Alexander N. Beecher and Xiaohao Yang contributed equally.

Notes

The authors declare no competing financial interest.

■ ACKNOWLEDGMENTS

We thank Dr. Joshua Choi for assistance with PDF measurements, Ava Kreider-Mueller and Prof. Gerard Parkin for assistance with SCXRD, Paul Kowalski of Bruker for assistance with LDI-MS analysis, Zachariah Norman for helpful discussions, Ruth Pachter for sharing coordinates of computed magic size clusters, and Paul Mulvaney and Jacek Jasieniak for sharing size-dependent optical data. Work on QD synthesis and growth kinetics was supported by the National Science Foundation through contract number NSF-CHE-1151172. PDF measurements were supported by the Center for Re-Defining Photovoltaic Efficiency Through Molecule Scale Control, an Energy Frontier Research Center funded by the U.S. Department of Energy, Office of Science, Office of Basic Energy Sciences under Award Number DE-SC0001085. PDF simulations and structure reliability studies were funded by Laboratory Directed Research and Development (LDRD) Program 12-007 (Complex Modeling) at the Brookhaven National Laboratory. X-ray experiments were carried out at the National Synchrotron Light Source, Brookhaven National Laboratory, which is supported by the U.S. Department of Energy, Division of Materials Sciences and Division of Chemical Sciences, DE-AC02-98CH10886. We thank the National Science Foundation (CHE-0619638) for the acquisition of an X-ray diffractometer.

■ REFERENCES

(1) Murray, C. B.; Norris, D. J.; Bawendi, M. G. *J. Am. Chem. Soc.* **1993**, *115*, 8706.
(2) Alivisatos, A. P. *Science* **1996**, *271*, 933.
(3) Billinge, S. J. L.; Levin, I. *Science* **2007**, *316*, 561.
(4) Jadzinsky, P. D.; Calero, G.; Ackerson, C. J.; Bushnell, D. A.; Kornberg, R. D. *Science* **2007**, *318*, 430.
(5) Desireddy, A.; Conn, B. E.; Guo, J.; Yoon, B.; Barnett, R. N.; Monahan, B. M.; Kirschbaum, K.; Griffith, W. P.; Whetten, R. L.; Landman, U.; Bigioni, T. P. *Nature* **2013**, *501*, 399.
(6) Juhás, P.; Cherba, D. M.; Duxbury, P. M.; Punch, W. F.; Billinge, S. J. L. *Nature* **2006**, *440*, 655.
(7) Young, C. A.; Goodwin, A. L. *J. Mater. Chem.* **2011**, *21*, 6464.
(8) Chen, O.; Zhao, J.; Chauhan, V. P.; Cui, J.; Wong, C.; Harris, D. K.; Wei, H.; Han, H.-S.; Fukumura, D.; Jain, R. K.; Bawendi, M. G. *Nat. Mater.* **2013**, *12*, 445.
(9) Kasuya, A.; Sivamohan, R.; Barnakov, Y. A.; Dmitruk, I. M.; Nirasawa, T.; Romanyuk, V. R.; Kumar, V.; Mamykin, S. V.; Tohji, K.; Jeyadevan, B.; Shinoda, K.; Kudo, T.; Terasaki, O.; Liu, Z.; Belosludov, R. V.; Sundararajan, V.; Kawazoe, Y. *Nat. Mater.* **2004**, *3*, 99.
(10) El-Sayed, M. A. *Acc. Chem. Res.* **2004**, *37*, 326.
(11) Bowers, M. J.; McBride, J. R.; Rosenthal, S. J. *J. Am. Chem. Soc.* **2005**, *127*, 15378.
(12) Cossairt, B. M.; Owen, J. S. *Chem. Mater.* **2011**, *23*, 3114.
(13) Cossairt, B. M.; Juhas, P.; Billinge, S. J. L.; Owen, J. S. *J. Phys. Chem. Lett.* **2011**, *2*, 3075.
(14) Yang, X.; Masadeh, A. S.; McBride, J. R.; Božin, E. S.; Rosenthal, S. J.; Billinge, S. J. L. *Phys. Chem. Chem. Phys.* **2013**, *15*, 8480.
(15) Dance, I. G.; Choy, A.; Scudder, M. L. *J. Am. Chem. Soc.* **1984**, *106*, 6285.
(16) Herron, N.; Calabrese, J. C.; Farneth, W. E.; Wang, Y. *Science* **1993**, *259*, 1426.
(17) Vossmeyer, T.; Reck, G.; Katsikas, L.; Haupt, E. T. K.; Schulz, B.; Weller, H. *Science* **1995**, *267*, 1476.
(18) Soloviev, V. N.; Eichhöfer, A.; Fenske, D.; Banin, U. *J. Am. Chem. Soc.* **2000**, *122*, 2673.
(19) Soloviev, V. N.; Eichhöfer, A.; Fenske, D.; Banin, U. *J. Am. Chem. Soc.* **2001**, *123*, 2354.
(20) Owen, J. S.; Park, J.; Trudeau, P. E.; Alivisatos, A. P. *J. Am. Chem. Soc.* **2008**, *130*, 12279.
(21) Fritzinger, B.; Capek, R. K.; Lambert, K.; Martins, J. C.; Hens, Z. *J. Am. Chem. Soc.* **2010**, *132*, 10195.
(22) Kudera, S.; Zanella, M.; Giannini, C.; Rizzo, A.; Li, Y.; Gigli, G.; Cingolani, R.; Ciccarella, G.; Spahl, W.; Parak, W. J.; Manna, L. *Adv. Mater.* **2007**, *19*, 548.
(23) Evans, C. M.; Love, A. M.; Weiss, E. A. *J. Am. Chem. Soc.* **2012**, *134*, 17298.
(24) Norris, D. J.; Bawendi, M. G. *Phys. Rev. B* **1996**, *53*, 16338.
(25) Klein, M. C.; Hache, F.; Ricard, D.; Flytzanis, C. *Phys. Rev. B* **1990**, *42*, 11123.
(26) Efros, A. L.; Ekimov, A. I.; Kozlowski, F.; Petrova-Koch, V.; Schmidbaur, H.; Shumilov, S. *Solid State Commun.* **1991**, *78*, 853.
(27) Scamarcio, G.; Spagnolo, V.; Ventruti, G.; Lugará, M.; Righini, G. C. *Phys. Rev. B* **1996**, *53*, R10489.
(28) Turro, N. J.; Ramamurthy, V.; Scaiano, J. C. *Modern molecular photochemistry of organic molecules*; University Science Books: Sausalito, Calif., 2010.
(29) Song, K. S.; Williams, R. T. *Self-Trapped Excitons*; Springer Series in Solid-State Sciences; Springer-Verlag: New York, 1993; Vol. *105*.
(30) Nguyen, K. A.; Day, P. N.; Pachter, R. *J. Phys. Chem. C* **2010**, *114*, 16197.
(31) Nguyen, K. A.; Pachter, R.; Day, P. N. *J. Chem. Theory Comput.* **2013**, *9*, 3581.
(32) Wang, Y.; Liu, Y.-H.; Zhang, Y.; Wang, F.; Kowalski, P. J.; Rohrs, H. W.; Loomis, R. A.; Gross, M. L.; Buhro, W. E. *Angew. Chem., Int. Ed.* **2012**, *51*, 6154.
(33) Vossmeyer, T.; Reck, G.; Schulz, B.; Katsikas, L.; Weller, H. *J. Am. Chem. Soc.* **1995**, *117*, 12881.
(34) Eichhöfer, A. *Eur. J. Inorg. Chem.* **2005**, *2005*, 1245.
(35) Anderson, N. C.; Hendricks, M. P.; Choi, J. J.; Owen, J. S. *J. Am. Chem. Soc.* **2013**, *135*, 18536.
(36) Lüth, H.; Nyburg, S. C.; Robinson, P. M.; Scott, H. G. *Mol. Cryst. Liq. Cryst.* **1974**, *27*, 337.
(37) Jasieniak, J.; Smith, L.; van Embden, J.; Mulvaney, P.; Califano, M. *J. Phys. Chem. C* **2009**, *113*, 19468.
(38) Wang, F.; Richards, V. N.; Shields, S. P.; Buhro, W. E. *Chem. Mater.* **2014**, *26*, 5.
(39) Hendricks, M. P.; Cossairt, B. M.; Owen, J. S. *ACS Nano* **2012**, *6*, 10054.
(40) Detty, M. R.; Seidler, M. D. *J. Org. Chem.* **1982**, *47*, 1354.
(41) Shannon, R. D. *Acta Crystallogr., Sect. A* **1976**, *32*, 751.

(42) Sheldrick, G. M. *SHELXTL*, An Integrated System for Solving, Refining and Displaying Crystal Structures from Diffraction Data; University of Göttingen, Göttingen, Federal Republic of Germany, 1981.
(43) Sheldrick, G. M. *Acta Crystallogr., Sect. A* **2008**, *64*, 112.
(44) Spek, A. L. *PLATON*, A Multipurpose Crystallographic Tool, Utrecht University, Utrecht, The Netherlands, 2005.
(45) Spek, A. L. *J. Appl. Crystallogr.* **2003**, *36*, 7.
(46) Wu, T.; Zhang, Q.; Hou, Y.; Wang, L.; Mao, C.; Zheng, S.-T.; Bu, X.; Feng, P. *J. Am. Chem. Soc.* **2013**, *135*, 10250.
(47) Zheng, N.; Bu, X.; Wang, B.; Feng, P. *Science* **2002**, *298*, 2366.
(48) Chupas, P. J.; Qiu, X.; Hanson, J. C.; Lee, P. L.; Grey, C. P.; Billinge, S. J. L. *J. Appl. Crystallogr.* **2003**, *36*, 1342.
(49) Yang, X.; Juhas, P.; Billinge, S. J. L. arXiv:1309.3614, 2013.
(50) Juhás, P.; Davis, T.; Farrow, C. L.; Billinge, S. J. L. *J. Appl. Crystallogr.* **2013**, *46*, 560.
(51) Egami, T.; Billinge, S. J. L. *Underneath the Bragg Peaks: Structural Analysis of Complex Materials*; Pergamon Materials Series, Second.; Elsevier: Amsterdam, 2012; Vol *16*.